Journal of Materials Chemistry A

Accepted Manuscript

ROYAL SOCIETY OF CHEMISTRY

www.rsc.org/materialsA

Journal Name

COMMUNICATION

A facile solution approach to photocatalytic active W, N co-doped TiO_2 nanobelt thin films†

Received 00th January 20xx,
Accepted 00th January 20xx

DOI: 10.1039/x0xx00000x

www.rsc.org/

Lu-Lu Lai[a] and Jin-Ming Wu[a]*

Hydrogen titanate nanobelt thin films were fabricated by oxidizing Ti plates with H_2O_2 solutions containing H_2WO_4 and $C_3H_6N_6$ at 80 °C. A subsequent calcination achieved W, N co-doped TiO_2 nanobelts, which possessed a band gap of 2.3 eV and high photocatalytic activity under both UV and visible light illumination.

For decades, semiconductors have found wide applications in thin film solar cells [1], Li-ion batteries [2] and water remediation [3], of which titanium dioxide (TiO_2) attracts the most attention [4,5]. Owing to its merits of environmental benign, chemical inertness, high stability, non-toxicity, low cost, and the ability to degrade a wide range of toxic and organic pollutants, TiO_2 has been vastly investigated as an effective photocatalyst [6]. The large nuisance for TiO_2 photocatalysis is that TiO_2 can be activated only under UV light owing to its wide band gap of 3.0-3.2 eV [7]. This weakness limits its applications and overall efficiency under the illumination of natural sunlight, which consists of a limited proportion of UV light for no more than 5 %. Visible light responsive TiO_2 photocatalysts are thus of urgent demands.

Visible light photocatalytic activity can be achieved by doping TiO_2 with transition metals [8] and non-metal elements [9]. Doping TiO_2 with non-metal ions like N, I, and S modifies its electronic structure by substituting the lattice oxygen to reconstruct the valence band so as to shift the adsorption edge to the visible light region [10]. Among them, N stands out as the most promising and frequently investigated candidate owing to its comparable ionic radius with O; however, N-doping has inherent drawbacks [11]. For example, the N-doping sites serve as charge recombination centres [12]. Increased trapping rate [13] and decreased charge carrier density [14] are also observed in the N-doped TiO_2. Co-doping with other metal and/or non-metal elements has been developed to overcome such drawbacks. In theory, the co-dopant should possess excess positive charges to compensate the excess negative charges brought by the doped nitrogen species. This can be obtained by doping with metal ions having a charge of 5^+ or more, among which W is a candidate [11]. The co-dopants of metal and non-metal can also reconstruct the conduction and valence band of TiO_2 simultaneously to narrower the band gap [15]. The W, N co-doped TiO_2 was demonstrated to exhibit high visible light activity by Thind *et al.* [16]. Cui *et al.* utilized ammonium metatungstate as the nitrogen and tungstate sources and synthesized W, N co-doped TiO_2 nanorods through a hydrothermal method, which demonstrated also a high visible light photocatalytic activity [17].

Compared with isotropic shapes such as nanoparticles, anisotropic shapes like nanorods, nanobelts, and nanowires have been found to enhance the efficiency of TiO_2 by possessing a comparatively lower charge-carrier recombination rate [18]. Vast literatures have been devoted to one-dimensional (1D) TiO_2 nanorods [19,19], 1D nanowires [21], and 3D nanoflowers [22]. Nanobelts integrate the merits of 2D nanomaterials with enhanced charge transport that is characteristic of 1D configuration, which hence attracted much attention in recent years. The synthesis of TiO_2 nanobelts is generally limited to hydrothermal routes [23,24], which involve subcritical water in a high pressure apparatus. In addition, nanobelts synthesized by hydrothermal methods often possess large dimensions, which reduce the effective catalyst surface and active sites, consequently lowering the efficiency of TiO_2. The hydrothermally synthesized TiO_2 nanobelts have been coupled with reduced graphene oxide [25], oxides [26,27], and sulphides [28] to enhance successfully the photocatalytic performance.

[a] State Key Laboratory of Silicon Materials and School of Materials Science and Engineering, Zhejiang University, Hangzhou, 310037, P. R. China. E-mail: msewjm@zju.edu.cn; Fax: +86 571 87953115; Tel: +86 571 87953115

† Electronic Supplementary Information (ESI) available: Experimental details, additional FESEM images, XRD patterns, Raman spectrum, UV-vis DRS spectrum, PL spectra, and photodegradation curves to support the discussion. See DOI: 10.1039/x0xx00000x

Qiao *et al.* developed a microwave-induced solid-state process to synthesize metastable TiO_2 (B) nanobelts with width of 30-100 nm and length up to a few microns [29]. However, the precursor utilized for the microwave treatment was synthesized also through an alkaline hydrothermal process [30]. Recently, Chen *et al.* synthesized TiO_2 nanobelts by electrochemical anodization of Ti in an electrolyte of water, NH_4F, and ethylene glycol [31]. The solution combustion of glycine, titanium oxysulfate-sulfuric acid hydrate and nitric acid resulted in a water-proof precursor, which reacted with H_2O_2 to form ultra-thin hydrogen titanate nanobelts and then to anatase nanobelts after a further calcination at 400 °C [32]. Other non-hydrothermal approaches to TiO_2 nanobelts include chemical vapor deposition [33] and laser direct writing in combination with etching [34].

In this work, we report a non-hydrothermal synthesis of W, N co-doped TiO_2 nanobelt thin film by a direct reaction between metallic Ti plate and H_2O_2 solution containing melamine ($C_3H_6N_6$) and H_2WO_4 at a low temperature of 80 °C for 72 h, followed by a subsequent calcination in air at 450 °C for 1 h (see ESI for experimental details). The band gap of TiO_2 was reduced effectively to *ca.* 2.3 eV. Under either UV or visible light illumination, the photocatalytic activity of the W, N co-doped TiO_2 nanobelt thin films is significantly higher than that synthesized by the generally adopted alkali-hydrothermal technique.

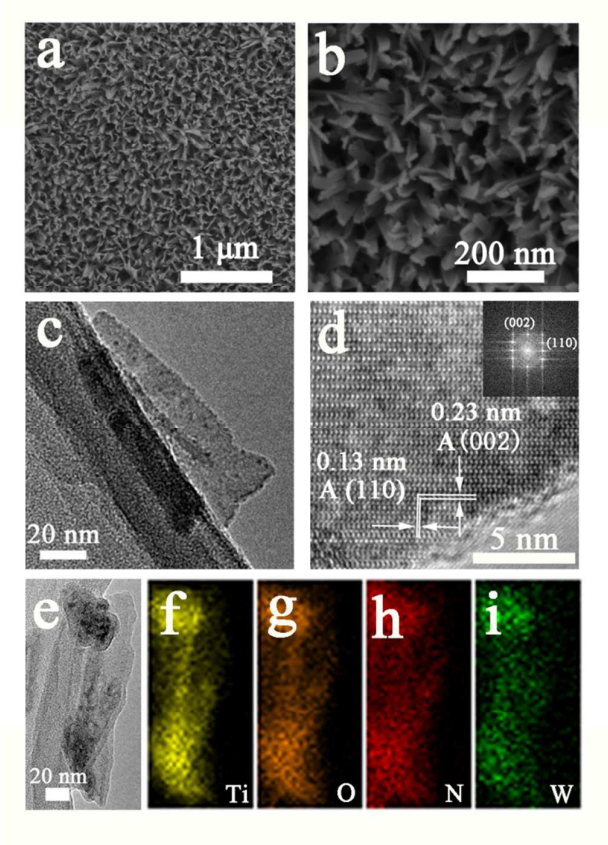

Figure 1. (a) Low and (b) high magnification FESEM images of the TiO_2 nanobelt film; (c) TEM and (d) HRTEM images of a TiO_2 nanobelt; (e) TEM image of another TiO_2 nanobelt and the corresponding EDS mapping images of (f) Ti, (g) O, (h) N, and (i) W. The inset in (d) presents the corresponding FFT pattern.

Figure 1a, b show the quasi-aligned nanobelts on the surface of the metallic Ti plate when subjected to oxidation at 80 °C for 72 h with H_2O_2 solution containing melamine and H_2WO_4, after a subsequent calcination in air at 450 °C for 1 h. The average width and length of the nanobelts is *ca.* 40 nm and 200 nm, respectively. Fig. 1c shows the TEM image of a nanobelt that is 35 nm in width and 100 nm in length. The corresponding HRTEM image demonstrates a set of perpendicular lattice fringes. The distance between the neighbouring lattice fringes, 0.23 and 0.13 nm, can be assigned to (002) and (110) of anatase TiO_2, respectively. The EDS mapping suggests the homogeneous distributions of Ti, O, N, and W elements throughout the nanobelt (Figs. 1e-i).

Figure 2a illustrates the XRD patterns of the nanobelts before and after calcination at 450 °C for 1 h in air. The as-synthesized nanobelts could be indexed to pentatitanate $H_2Ti_5O_{11}\cdot 3H_2O$ (JCPDS card 44-0130) by showing a strong diffraction peak at 2ϑ=8.4°. The subsequent calcination decomposed the pentatitanate to anatase (JCPDS card 21-1272). The Raman spectrum of the calcinated nanobelts shows peaks located at 146.4, 296.3, 516.0, and 638.5 cm^{-1}, which could be attributed to the anatase TiO_2 (Fig. 2b) [35].

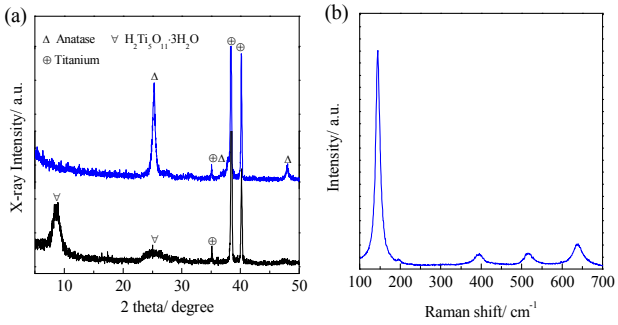

Figure 2. (a) XRD patterns of the nanobelt film before and after calcination in air at 450 °C for 1 h; (b) Raman spectrum of the calcinated TiO_2 nanobelt film.

The transition temperature from hydrogen titanate to TiO_2 is dependent on the fabrication history, which affects readily the titanate type and also the impurity. Zhou et al. reported that, the alkali-hydrothermally derived $H_2Ti_3O_7$ nanobelts decomposed to TiO_2 (B) after the subsequent calcination at 400 °C, which transformed to anatase TiO_2 upon calcinations at higher temperatures of 600-900 °C [36]; however, an alkali-hydrothermally synthesized titanate nanobelt film was reported to decompose to anatase TiO_2 at a much lower temperature of 450 °C [37]. The relatively low temperature required to fulfill the transition may also be attributed to the sodium-free feature of the titanate gained in the current work [32].

The high-resolution Ti 2p, O 1s, N 1s, and W 4f XPS spectra of the calcinated nanobelt film are shown in Fig. 3. There are two peaks in

the Ti 2p region. The peak located at 464.0 eV corresponds to Ti $2p_{1/2}$ and the other peak located at 458.3 eV is assigned to Ti $2p_{3/2}$. The splitting between Ti $2p_{1/2}$ and Ti $2p_{3/2}$ is 5.7 eV, which is characteristic of Ti^{4+} [38]. The O 1s spectrum can be fitted into two peaks. The lower binding energy (BE) peak located at 529.6 eV originated from lattice oxygen (Ti-O or W-O) and the higher BE peak located at 530.7 eV can be assigned to the hydroxyl groups (-OH) [39]. The N 1s spectrum can be fitted into three peaks located at 398.7, 399.3, and 401.2 eV, respectively. The peaks at 398.7 and 399.3 eV can be attributed to the incorporated nitrogen as interstitial N or O-Ti-N, indicating that N has been incorporated into TiO_2 successfully; whilst the peak at 401.2 eV corresponds to the surface-adsorbed or contaminated nitrogen species [40]. Fig. 3d displays W $4f_{7/2}$ and $4f_{5/2}$ peaks at 34.8 and 36.8 eV. The splitting of the 4f doublet of W is 2.0 eV, indicating a state of W^{6+}. For pure WO_3, the typical W $4f_{7/2}$ and $4f_{5/2}$ peaks locate at 35.3 and 37.4 eV [41]. The shift in BE can be attributed to the formation of W-O-Ti bonds in the framework of TiO_2, indicating the successful doping of W. The other peak located at 37.0 eV in Fig. 3d comes from the Ti 3p state [15]. The XPS spectra, together with the EDS mapping, well demonstrate that the TiO_2 nanobelt films synthesized in current investigation are co-doped with W and N. The atomic concentrations of W and N estimated by the XPS measurement were 2.6 % and 3.1 %, respectively.

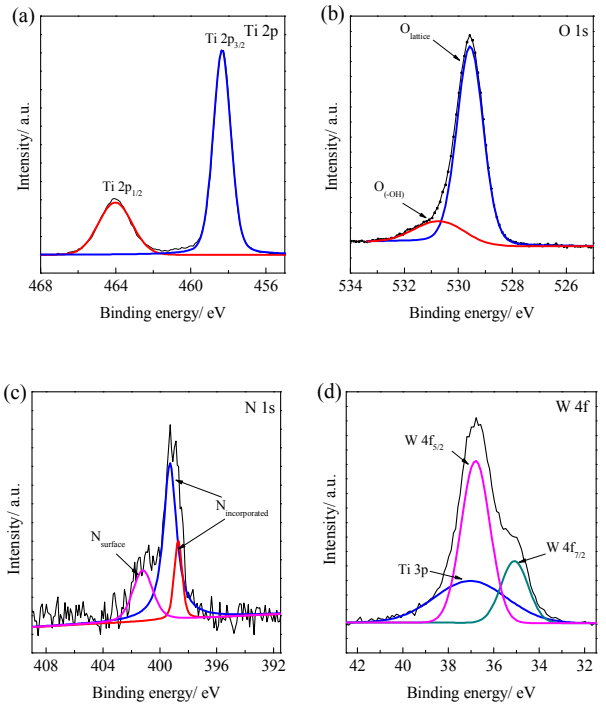

Figure 3. High-resolution XPS spectra of (a) Ti 2p, (b) O 1s, (c) N 1s, and (d) W 4f for the TiO_2 nanobelt film.

To better understand the formation process of the nanobelt structure, the morphology evolution upon the reaction duration was investigated (Fig. S1). Only nanowires can be observed after reactions of 6 h (Fig. S1a, b) and 12 h (Fig. S1c, d). Further increasing the reaction time to 24 h, belt-like structure appeared, coexisting with nanowires (Fig. S1e, f). Once the reaction time reached 48 h, the substrate was covered homogenously with quasi-aligned nanobelts with an average width of 35 nm (Fig. S1g, h). The XRD patterns revealed that the nanowires were also pentatitanate $H_2Ti_5O_{11}\cdot 3H_2O$ (Fig. S2).

The formation of the pentatitanate nanobelts can thus be explained based on a dissolution/precipitation mechanism. The Ti plate was gradually corroded by H_2O_2, which released Ti(IV) ions into the solution. Because of the limited solubility of Ti(IV) ions in water, hydrated Ti(IV) ions saturated easily, which led to the precipitation of pentatitanate nanowires at the early stage. Afterwards, the nanowires grew along the horizontal direction and further grew into nanobelts. The subsequent thermal treatment in air decomposed the pentatitanate to anatase TiO_2, with the nanobelt morphology well preserved. Though H_2WO_4 has limited solubility in water, it can form a stable peroxocomplex with H_2O_2 [42], which would be involved in the dissolution and precipitation process and in turn achieved the W-doping into the framework of the pentatitanate. The hydrolysis products of melamine, which possesses hydroxyl groups, will bind to the framework during the reaction to fulfill the N-doping [38].

The additives of both melamine and H_2WO_4 are indispensible for the formation of the present TiO_2 nanobelts. The oxidation of Ti plate in H_2O_2 solution at 80 °C for 72 h achieved quasi-aligned TiO_2 nanorods (Fig. S3a, b) [43]. With the additive of melamine, thin films of nanoflakes were gained (Fig. S3c, d); while adding solely H_2WO_4 into the H_2O_2 solution achieved thin films of fused nanowires (Fig. S3e, f). The XRD patterns (Fig. S4) show that the TiO_2 thin film derived with pure H_2O_2 is a mixture of anatase and rutile. With the additive of either melamine or H_2WO_4 in the H_2O_2 solution, only anatase TiO_2 was achieved after the final calcination.

As illustrated by the UV-Vis diffuse reflectance spectrum in Fig. 4, the absorption edge of the present W, N co-doped anatase TiO_2 nanobelts shifted from UV to visible light region. The band gap is determined to be *ca.* 2.33 eV, which is much lower than the bulk TiO_2 (3.2 eV for anatase and 3.0 eV for rutile) [44]. The reduced band gap for TiO_2 nanobelts is attributed to the co-doping of W and N, which introduced both the narrow substitute N 2p band that formed above the O 2p valence band and the donor state for W^{6+}/W^{4+} that located under the conduction band of TiO_2 [17]. The calculation of W, N co-doping effect carried out by Marquez *et al.* based on anatase (101) surface pointed out that, the reduction of the band gap was mainly associated to a decrease of the lowest Ti 3d levels of the conduction band; and there was a midgap state appearing around 0.8 eV above the valence band, which was associated to N 2p and O 2p energy levels [45]. Bloh and co-workers demonstrated that W-doping was responsible for the change in the lattice parameter of TiO_2 and the facilitation of N-doping; whilst N-doping led to the formation of the mid-band gap and the shift of the conduction band [46].

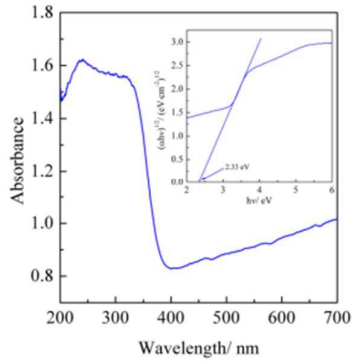

Figure 4. UV-Vis diffuse reflectance spectrum of the TiO_2 nanobelt film. The inset shows the spectrum in an $(\alpha h\nu)^{1/2}$ ~ hν coordinate to evaluate the corresponding band gap.

To evaluate the photocatalytic activity of the present W, N co-doped TiO_2 nanobelt film, aqueous rhodamine B solution was chosen as a model organic. TiO_2 nanobelt films synthesized via generally adopted alkali-hydrothermal technique were employed for comparisons. After the sequential treatments of alkali-hydrothermal at 180 °C for 24 h, proton exchange, and calcination in air at 450 ^{o}C for 1 h, anatase TiO_2 nanobelt film was achieved (Figs. S5 and S6). The nanobelts were *ca.* 300 nm in width (Fig S6) and the film thickness was *ca.* 8 μm (Fig. S7b). The band gap was determined to be *ca.* 2.84 eV (Fig. S8), which was lower than that of bulk anatase but significantly higher than the W, N co-doped TiO_2 nanobelt film achieved in the current investigation.

Figure 5 illustrates the photodegradation of rhodamine B in water, in the presence of the two TiO_2 nanobelt films and under the illumination of UV, visible, and UV+Vis light. All the degradation procedures can be fitted well by a pseudo-first order kinetic. The reaction rate constants are summarized in Table 1. In absence of any photocatalyst, the rhodamine B degradation is negligible despite of the different light sources used. The presence of the TiO_2 nanobelt films accelerated the photodegradation procedure (Fig. 5a, c and e). Under identical conditions, the W, N co-doped TiO_2 nanobelt film exhibited much higher activity than the alkali-hydrothermally synthesized one. Exposure of the dye solution to visible light for 4 h resulted in degradations of 93% and 59 % of rhodamine B molecules over the W, N co-doped TiO_2 nanobelt film and the alkali-hydrothermally synthesized one, respectively. The superior visible light activity of the W, N co-doped TiO_2 nanobelt film is owing to the co-doping effect, which greatly reduces the band gap value, and hence the enhanced absorbance in the visible light region. The tendency is similar under the illumination of UV light and UV+Vis light. With the assistance of UV light, the degradation efficiency of the W, N co-doped TiO_2 nanobelt film is improved. Under illumination of UV light and UV+Vis light, there remained 16% and 5% rhodamine B in water, respectively, after 2 h of the photodegradation. Within the same period, the alkali-hydrothermally synthesized TiO_2 nanobelt film can only degrade 47 % and 50 % rhodamine B molecules.

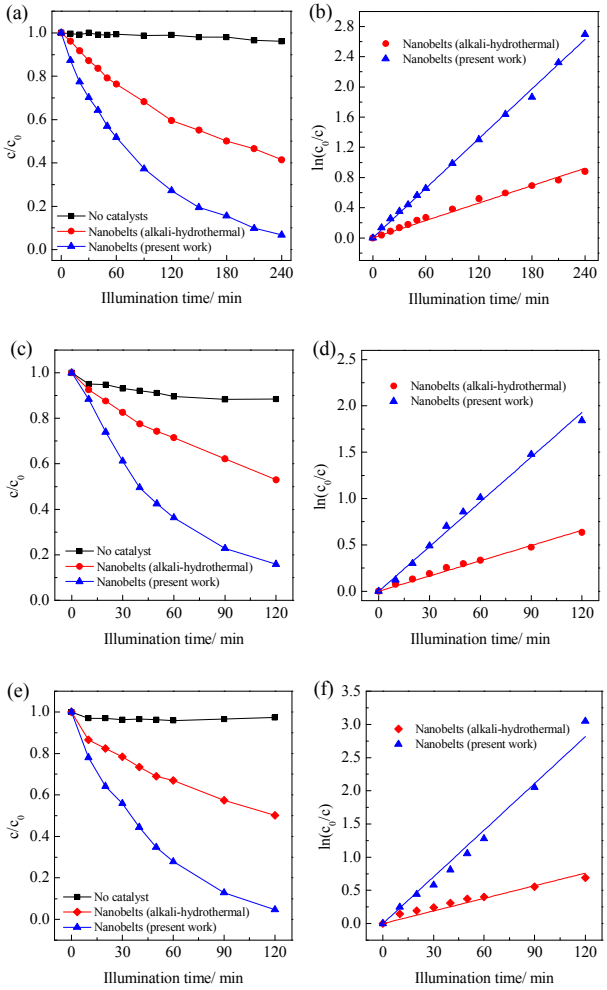

Figure 5. Photodegradation curves of rhodamine B in water in the presence of different catalysts under (a) visible light, (c) UV light, and (e) UV+Vis light; (b, d, f) represent the corresponding fitting results assuming a pseudo-first order reaction.

Doping TiO_2 usually results in more charge recombination centres which lead to reduced photocatalytic activity under UV light illumination. In the current investigation, the photocatalytic activity of the W, N co-doped TiO_2 nanobelt is still superior to that of the alkali-hydrothermally derived un-doped TiO_2 nanobelt. This can be contributed to the much thinner belts, which reduced the charge migration length, increased the catalyst surface and active sites.

To have a deeper understanding of the reason leading to the distinct photocatalytic activity, PL tests were carried out for both films (Fig. S9). The W, N co-doped TiO_2 nanobelt film exhibited a weaker PL intensity than that derived by the alkali-hydrothermal route, implying a lower charge recombination rate, which can be attributed to the smaller dimensions when compared with alkali-hydrothermally synthesized nanobelts. When compared with the anatase TiO_2 film achieved by adding solely melamine in the H_2O_2 solution, the PL intensity of the W, N co-doped TiO_2 nanobelt film is

Table 1 Reaction rate constants (k) for the photodegradation of rhodamine B in water in the presence of the TiO_2 nanobelt films fabricated by the alkali-hydrothermal treatment and the present solution approach, under the various light sources.

Light source	Intensity $mW \cdot cm^{-2}$	k (Nanobelts, alkali-hydrothermal) $\times 10^{-3}$ min^{-1}	k (Nanobelts, present solution approach) $\times 10^{-3}$ min^{-1}
Visible light	190	3.85	11.0
UV light	4.5	5.40	16.1
Xenon light	UV: 4.5; Vis: 190	6.33	23.5

also much weaker, which evidenced the enhanced contributions of the W, N co-doping to the reduced charge recombination. The comparison in PL intensity for the two films with distinct thickness is meaningful because a compact TiO_2 film 200 nm in thickness would adsorb nearly 100% intensity of the exciting UV light with a wavelength of 300 nm ($\alpha\ (TiO_2)_{300} = 3.5 \times 10^5\ cm^{-1}$) [47].

Figure 6 shows the photodegradation curves of rhodamine B under the UV+Vis light illumination and in the presence of the TiO_2 thin films fabricated using pure H_2O_2, H_2O_2 with the additive of melamine only, with H_2WO_4 only, and both (refer to Fig. S3 for the morphology and Fig. S4 for the phase composition). The un-doped TiO_2 exhibited the lowest photocatalytic activity by degrading 28 % rhodamine B molecules within 2 h. The single N-doped, W-doped, and W, N co-doped TiO_2 induced photodegradations of 88 %, 73 % and 95% rhodamine B molecules, respectively. The higher activity of the W, N co-doped TiO_2 when compared with single element doping further supports the positive synergetic effects arising from the co-doping tactic.

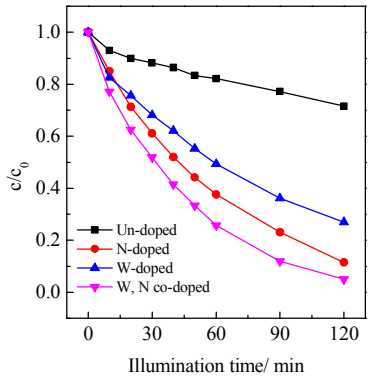

Figure 6. Photodegradation curves of rhodamine B aqueous solution under the UV+Vis light illumination, in the presence of different TiO_2 thin films: un-doped, single N-doped, single W-doped, and W, N co-doped.

The stability of the W, N co-doped TiO_2 nanobelt film was confirmed by repetitively degradations of rhodamine B in water under the illumination of the UV+Vis light for up to 10 cycles (Fig. S10). Considering the easily scale-up of the one-pot and non-hydrothermal synthesis, the W, N co-doped TiO_2 nanobelt film reported herein may find potential applications in photocatalysis, and also the various fields of thin film solar cells and Li-ion batteries.

Conclusions

W, N co-doped TiO_2 nanobelt films were synthesized through a facile and low temperature route followed by a subsequent calcination. With the additive of H_2WO_4 and melamine in the aqueous H_2O_2 solution, thin films of pentatitanate $H_2Ti_5O_{11} \cdot 3H_2O$ nanobelts were deposited directly on the metallic Ti substrates when maintained at 80 °C for 72 h. The subsequent calcination in air at 450 °C for 1 h decomposed the pentatitanate to anatase TiO_2, with the nanobelt morphology well retained. The achieved anatase TiO_2 nanobelt film possessed a much reduced band gap of *ca.* 2.3 eV when compared with bulk anatase, thanks to the co-doping of *ca.* 2.6 at. % W and 3.1 at. % N. The nanobelt structure along with the co-doping effect guaranteed an excellent performance of TiO_2 when utilized to assist the photodegradation of rhodamine B in water, under the illumination of either UV or visible light.

Acknowledgements

This work is funded by Zhejiang Provincial Natural Science Foundation of China under Grant No. LY13E020001, and Department of Science and Technology of Zhejiang Province under Contract No. 2015C31034.

Notes and references

1 C.H. Lee, W.H. Chiu, K.M. Lee, W.F. Hsieh, J.M. Wu, *J. Mater. Chem.*, 2011, **21**, 5114.
2 J.S. Chen, Y.L. Tan, C.M. Li, Y.L. Cheah, D.Y. Luan, S. Madhavi, F.Y.C. Boey, A. Archer, X.W. Lou, *J. Am. Chem. Soc.*, 2010, **132**, 6124.
3 Q. Li, N. Zhang, Y. Yang, G.Z. Wang and D.H.L. Ng, *Langmuir,* 2014, **30**, 8965.
4 S.W. Liu, J.G. Yu, M. Jaroniec, *J. Am. Chem. Soc.*, 2010, **132**, 11914.
5 W.J. Zhou, H. Liu, R.I. Boughton, G.J. Du, J.J. Lin, J.Y. Wang, D. Liu, *J. Mater. Chem.*, 2010, **20**, 5993.
6 S. Okunaka, H. Tokudome, Y. Hitomi and R. Abe, *J. Mater. Chem. A*, 2015, **3**, 1688.
7 J. Wang, D.N. Tafen, J.P. Lewis, Z.L. Hong, A. Manivannan, M.J. Zhi, M. Li and N.Q. Wu, *J. Am. Chem. Soc.*, 2009, **313**, 12290.
8 N. Roy, Y.K. Sohn, K.T. Leung, D. Pradhan, *J. Phys. Chem. C*, 2014, **118**, 29499.
9 R. Asahi, T. Morikawa, H. Irie, T. Ohwaki, *Chem. Rev.,* 2014, **114**, 9824.
10 T.Q. Lin, C.Y. Yang, Z. Wang, H. Yin, X.J. Lu, F.Q. Huang, J.H. Lin, X.M. Xie, M.H. Jiang, *Energy Environ. Sci.*, 2014, **7**, 967.
11 J.Z. Bloh, A. Folli, D.E. Macphee, *J. Phys. Chem. C*, 2014, **118**, 21281.

12 H. Irie, Y. Watanabe, K. Hashimoto, *J. Phys. Chem. B,* 2003, **107**, 5483.
13 R. Katoh, A. Furube, K. Yamanaka, T. Morikawa, *J. Phys. Chem. Lett.,* 2010, **1**, 3261.
14 K. Yamanaka, T. Morikawa, *J. Phys. Chem. C*, 2012, **116**, 1286.
15 J.Y. Gong, W.H. Pu, C.Z. Yang, J.D. Zhang, *Chem. Eng. J.,* 2012, **209**, 94.
16 S.S. Thind, G.S. Wu, A.C. Chen, *Appl. Catal. B Environ.,* 2012, **111-112**, 38.
17 X.Y. Cui, S.Z. Rong, Y.L. Cao, Y.K. Yin, S.J. Li, M.J. Li, *Appl. Phys. A*, 2013, **113**, 47.
18 M. D'Arienzo, J. Carbajo, A. Bahamonde, M. Crippa, S. Polizzi, R. Scotti, L. Wahba, F. Morazzoni, *J. Am. Chem. Soc.,* 2011, **133**, 17652.
19 J.M. Wu, T.W. Zhang, Y.W. Zeng, S. Hayakawa, K. Tsuru, A. Osaka, *Langmuir,* 2005, **21**, 6995.
20 D.H. Kim, W.M. Seong, I.J. Park, E.S. Yoo, S.S. Shin, J.S. Kim, H.S. Jung, S. Lee, K.S. Hong, *Nanoscale,* 2015, **5**, 11725.
21 P. Sudhagar, A. Devadoss, T. Song, P. Lakshmipathiraj, H. Han, V.V. Lysak, C. Terashima, K. Nakata, A. Fujishima, U. Paik, Y.S. Kang, *Phys. Chem. Chem. Phys.,* 2014, **16**, 17748.
22 X.F. Yang, C.J. Jin, C.L. Liang, D.H. Chen, M.M. Wu, J.C. Yu, *Chem. Comm*., 2011, **47**, 1184.
23 D. Sarkar, K.K. Chattopadhyay, *Appl. Mater. Interfaces*, 2014, **6**, 10044.
24 W.J. Zhou, G.J. Du, P.G. Hu, G.H. Li, D.Z. Wang, H. Liu, J.Y. Wang, R.I. Boughton, D. Liu, H.D. Jiang, *J. Mater. Chem.,* 2011, **21**, 7937.
25 J.Y. Zhang, F.X. Xiao, G.C. Xiao, B. Liu, *Nanoscale*, 2014, **6**, 11293.
26 W.J. Zhou, H. Liu, J.Y. Wang, D. Liu, G.J. Du, J.J. Cui, *ACS Appl. Mater. Interfaces*, 2010, **2**, 2385.
27 W.J. Zhou, Y.H. Leng, D.M. Hou, H.D. Li, L.G. Li, G.Q. Li, H. Liu, S.W. Chen, *Nanoscale,* 2014, **6**, 4698.
28 W.J. Zhou, Z.Y. Yin, Y.P. Du, X. Huang, Z.Y. Zeng, Z.X. Fan, H. Liu, J.Y. Wang, H. Zhang, *Small*, 2013, **9**, 140.
29 Y. Qiao, X.L. Hu and Y.H. Huang, *J. Nanopart. Res.,* 2012, **14**, 684.
30 Y.M. Wang, G.J. Du, H. Liu, D. Liu, S.B. Qin, N. Wang, C.G. Hu, X.T. Tao, J. Jiao, J.Y. Wang, Z.L. Wang, *Adv. Funct. Mater.*, 2008, **18**, 1131.
31 Q.H. Chen, H.L. Liu, Y.J. Xin, X.W. Cheng, J. Zhang, J.J. Li, P. Wang, H.J. Li, *Electrochim. Acta*, 2013, **99**, 152.
32 W. Wen, J.M. Wu, Y.Z. Jiang, S.L. Yu, J.Q. Bai, M.H. Cao, J. Cui, *Sci. Rep.*, 2015, **5**, 11804.
33 N.T.Q. Hoa, E.T. Kim, *Electrochem. Solid-State Lett.,* 2008, **11**, K1.
34 Y.S. Wang, R. Wang, C.F. Guo, J.J. Miao, Y. Tian, T.L. Ren, Q. Liu, *Nanoscale,* 2012, **4**, 1545.
35 R.H. Zha, R. Nadimicherla, X. Guo, *J. Mater. Chem. A*, 2015, **3**, 6565.
36 W.J. Zhou, L.G. Gai, P.G. Hu, J.J. Cui, X.Y. Liu, D.Z. Wang, G.H. Li, H.D. Jiang, D. Liu, H. Liu, J.Y. Wang, *CrystEngComm*, 2011, **13**, 6643.
37 Y.S. Luo, J.S. Luo, W.W. Zhou, X.Y. Qi, H. Zhang, Y.W. Yu, C.M. Li, H.J. Fan, T. Yu, *J. Mater. Chem. A*, 2013, **1**, 273.
38 J.M. Wu, H.X. Xue, *J. Am. Ceram. Soc.,* 2009, **92**, 2139.
39 L. Zhang, Y.G. Li, Q.H. Zhang, H.Z. Wang, *CrystEngComm,* 2013, **15**, 5986
40 A.Y. Zhang, L.L. Long, C. Liu, W.W. Li, H.Q. Yu, *Green Chem.,* 2014, **16**, 2745.
41 S. Liu, E.Y. Guo, L.W. Yin, *J. Mater. Chem.*, 2012, **22**, 5031.
42 I.A. Castro, W. Avansi Jr, C. Ribeiro, *CrystEngComm*, 2014, **16**, 1514.
43 J.M. Wu, *Environ. Sci. Technol.*, 2007, **41**, 1723.
44 Y.C. Lan, Y.L. Lu, Z.F. Ren, *Nano Energy,* 2013, **2**, 1031.
45 A.M. Marquez, J.J. Plata, Y. Ortega, J.F. Sanz, *J. Phys. Chem. C*, 2012, **116**, 18759.
46 A. Kubacka, B.B. Baeza, G. Colon, M.F. Garcia, *Appl. Catal. B Environ.,* 2010, **93**, 274.
47 A. Mills, S. Lee, A. Lepre, I.P. Parkin, S.A. O'Neill, *Photochem. Photobiol. Sci.,* 2002, **1**, 865.

Table of Contents Entry

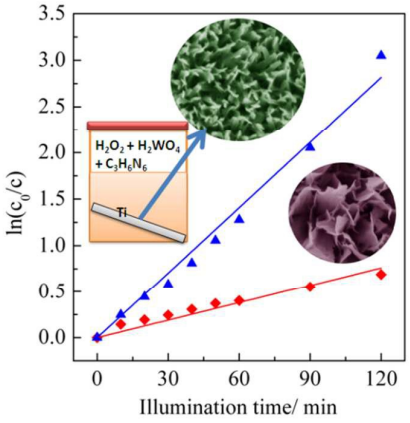

W, N co-doped anatase TiO_2 nanobelt films were synthesized by direct oxidation of metallic Ti substrates with H_2O_2 solutions containing H_2WO_4 and $C_3H_6N_6$ at 80 ºC, followed by a subsequent calcination. The photocatalytic activity of the W, N co-doped anatase TiO_2 nanobelt films was nearly three times that of undoped alkali-hydrothermal synthesized anatase TiO_2 nanobelt films, under the UV and visible light illumination.